Effect of Surface Modification on Nano-Structured $LiNi_{0.5}Mn_{1.5}O_4$ Spinel Materials

Hyung-Man Cho,[†,‡] Michael Vincent Chen,[†] Alex C. MacRae,[†,§] and Ying Shirley Meng[*,†,‡]

[†]Department of NanoEngineering, University of California San Diego, 9500 Gilman Drive, La Jolla, California 92093, United States
[‡]Materials Science and Engineering, University of California San Diego, 9500 Gilman Drive, La Jolla, California 92093, United States
[§]Department of Chemistry and Biochemistry, University of California, San Diego, 9500 Gilman Dr. La Jolla, California 92093-0358, United States

Ⓢ *Supporting Information*
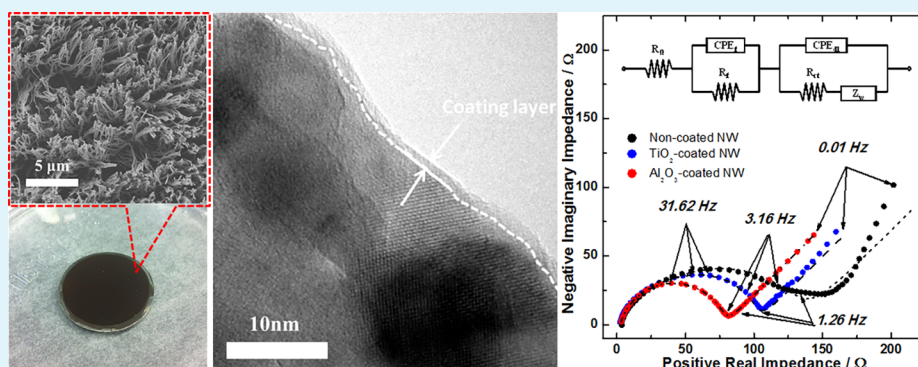
ABSTRACT: Fine-tuning of particle size and morphology has been shown to result in differential material performance in the area of secondary lithium-ion batteries. For instance, reduction of particle size to the nanoregime typically leads to better transport of electrochemically active species by increasing the amount of reaction sites as a result of higher electrode surface area. The spinel-phase oxide $LiNi_{0.5}Mn_{1.5}O_4$ (LNMO), was prepared using a sol−gel based template synthesis to yield nanowire morphology without any additional binders or electronic conducting agents. Therefore, proper experimentation of the nanosize effect can be achieved in this study. The spinel phase LMNO is a high energy electrode material currently being explored for use in lithium-ion batteries, with a specific capacity of 146 mAh/g and high-voltage plateau at ∼4.7 V (vs Li/Li^+). However, research has shown that extensive electrolyte decomposition and the formation of a surface passivation layer results when LMNO is implemented as a cathode in electrochemical cells. As a result of the high surface area associated with nanosized particles, manganese ion dissolution results in capacity fading over prolonged cycling. In order to prevent these detrimental effects without compromising electrochemical performance, various coating methods have been explored. In this work, TiO_2 and Al_2O_3 thin films were deposited using atomic layer deposition (ALD) on the surface of LNMO particles. This resulted in effective surface protection by prevention of electrolyte side reactions and a sharp reduction in resistance at the electrode/electrolyte interface region.

KEYWORDS: $LiNi_{0.5}Mn_{1.5}O_4$ spinel, nano-structured electrode, surface modification, ALD, cation dissolution

■ INTRODUCTION

Lithium-ion batteries have found nearly innumerable applications since their commercial release in 1991, providing energy for everything from portable electronic devices to electric vehicles.[1] Among cathode materials, $LiNi_{0.5}Mn_{1.5}O_4$ (LNMO) has received significant interest as a candidate for replacement of the currently commercialized cathode materials, ($LiCoO_2$) for lithium-ion batteries.[2,3] The operating voltage of LNMO is particularly high at ∼4.7 V (vs. Li/Li^+) while also providing a relatively high capacity (theoretical specific capacity: 146.72 mA h g^{-1}). Nevertheless, improvement of LNMO cathode materials is still of particular interest in order to produce batteries that meet the superior power performance required for transportation vehicles. Higher power output is directly correlated to lithium ion intercalation/deintercalation rates, which can be improved by particle size reduction of the active electrode material.[4−8]

The improvement of lithiation/delithiation kinetics can be ascribed to a sharp reduction in the characteristic time constant ($t = L^2/D$; L = diffusion length, D = diffusion constant). The time t for intercalation decreases with the square of the particle size upon reduction of micrometer dimensions. In addition, a large surface area permits extensive electrode−electrolyte contact, leading to a high lithium-ion flux across the interface.

As a result of the shortened electron pathway through the active electrode material, the electrical resistance of nanosized materials is significantly less than comparable micron-sized particles. The implementation of nanoparticulate electrode materials results in various benefits, however deleterious aspects can be intensified. For example, the increase in surface area results in an escalation in electrode−electrolyte side reactions. This phenomenon is augmented at both high (>4.3 V vs Li/Li⁺) and low (<1.0 V vs Li/Li⁺) operating potentials.[9] For this reason, most of previous nanostructured material research was limited to electrodes operating under low operating voltages, such as most of anodes,[10−12] LiFePO₄,[13] etc.

To overcome this common problem, surface modification of the material is required for stabilization of the interface between the electrolyte and electrode.[14−16] Recently, various materials have been investigated as possible coatings on the LiNi₀.₅Mn₁.₅O₄ electrodes. Metal oxide[15,17−22] and polymer[23,24] coatings have been employed as possible materials to prevent manganese dissolution. Carbon has been explored as an additive to both prevent dissolution, as well as increase electronic conductivity.[25] Various surface modification methods, such as physical vapor deposition or wet-chemical techniques have been utilized with the aim of improving interfacial properties. However, these methods have limitations that include nonconformity and unwanted phase transformations due to interdiffusion of the elements during high temperature operation. Unlike other surface modification methods, atomic layer deposition (ALD) is a particularly useful method for deposition of conformal thin films with a high degree of thickness variation.[26−30] The low temperature process implements a coating only at the surface, thereby preventing unpredictable changes in the bulk. While the use of ALD to deposit protective layers on conventional LNMO electrodes containing both carbon and binding additives has been reported,[21,22] there exists an absence of publications concerning electrodes without such additives. In the present study, the nanowire LNMO cathode material is prepared and probed without such additives, allowing for investigation of nanosize effects.

Prior studies indicate that strong deviation of electrochemical properties results when cathode particles are reduced from the micron-regime to that of the nano.[4,12] However, there remains a dearth of quantitative understanding of the degree that reduction to nanosize affects elementary electrochemical parameters. This work provides critical insights in the analysis of lithium-ion transport kinetics of nanostructured materials and analytical studies concerning ALD surface modifications to successively inhibit deleterious side-reactions. Following surface modification of the LNMO cathode material, the elementary resistances involved in cell operation have been quantitatively investigated.

■ EXPERIMENTAL SECTION

One-Dimensional Nanostructured (Nanowire) Electrode Fabrication. The spinel-phase material LiNi₀.₅Mn₁.₅O₄ with nanowire morphology was prepared using a sol−gel based template synthesis[31] (Figure 1a). A commercially available polycarbonate membrane with a nominal pore diameter of 200 nm (Whatman, P/N 7060-2502) was used as the template. The sol solution was prepared using a stoichiometric mixture of nickel acetate tetrahydrate (1.867 g), manganese acetate tetrahydrate (5.514 g), and lithium acetate diacetate (1.530 g) dissolved in deionized water (100 mL) with 0.5 wt % poly(vinyl alcohol) (PVA). All chemicals were purchased from Aldrich and used as received. The template filled with the as-prepared
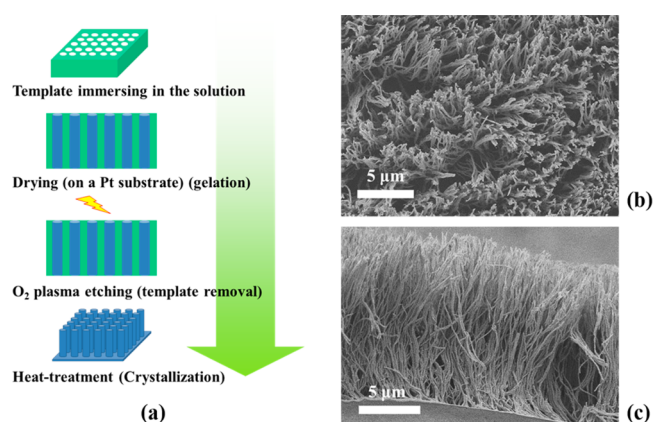

Figure 1. (a) Schematics of the sol−gel based template synthesis. Scanning electron micrographs of (b) top and (c) cross-sectional views of LiNi₀.₅Mn₁.₅O₄ nanowire electrode prepared via sol−gel based template synthesis method.

solution was placed on a Pt foil current collector and dried overnight at 70 °C. The template was removed using an oxygen plasma etching system (Trion RIE/ICP dry etcher) under the following operating conditions: 50 sccm O₂ flow rate, 100 mTorr O₂ pressure, 150 W RF power, and an etching time of 2 h. Finally, the nanowire electrode was crystallized at 800 °C for 1 h.

Atomic Layer Deposition (ALD). TiO₂ and Al₂O₃ thin films were deposited on the as-prepared nanowire electrodes using atomic layer deposition (Beneq TFS200). Titanium tetrachloride and water were used as the precursors for the TiO₂ deposition. Deposition of Al₂O₃ required the use of trimethylaluminum and water as precursor reagents. Both deposition experiments employed N₂ as the carrier gas and were carried out at 250 °C.

Materials Characterizations. Scanning electron microscope (SEM) (Phillips, XL30) and transmission electron microscope (TEM) (FEI Tecnai G2 Sphera cryo-electron microscope) were utilized in order to examine particle morphology and size distribution. The chemical composition was determined using an energy dispersive X-ray detector (EDX) equipped in the SEM. Crystallinity of the samples was examined by X-ray diffraction (XRD) (Bruker D8) with Cu Kα radiation. XRD data was gathered in the range of 2θ = 10−80°, at a scan rate of 0.02 deg s⁻¹. The refinement of the XRD data was carried out using the Rietveld method in the FullProf software package suite. The Ni/Mn molar ratio in the solid and electrolyte samples was characterized by inductively coupled plasma optical emission spectroscopy (ICP-OES) (PerkinElmer Plasma 3700). Twenty-five μL of electrolyte is collected from a custom-made electrochemical cell and added to a 25 mL solution matrix (1:1 wt %, HCl/HNO₃). Therefore, the electrolyte solution is tested at a 1000 times dilution.

Electrochemical Characterization. A custom-made three-electrode cell was employed for electrochemical experiments.[32−34] To remove the effect of the lithium metal counter electrode on the electrochemistry, a three-electrode cell configuration is necessary. This effect is reflected in impedance analysis, as the impedance from the counter electrode can influence the working electrode properties. As a result, we employed the three-electrode cell configuration for impedance experiments. For electrochemical experiments such as galvanostatic cycling and C-rate determination, a two electrode cell configuration was employed using the LMNO nanowire cathode and lithium metal anode. Nanostructured electrodes and lithium metal foil were used for the positive and negative electrodes, respectively. A 1 M solution of lithium hexafluorophosphate (LiPF₆) dissolved in a 50/50 (v/v) mixture of ethylene carbonate (EC) and dimethyl carbonate (DMC) was used as electrolyte. The electrochemical cells were assembled in an argon filled glovebox (MBraun) (H₂O concentration <1 ppm). The specific capacity in this work was calculated on the basis of the active mass of NW electrode. The mass of each electrode including Pt substrate was estimated statistically by measuring the

electrode mass ten times using a microbalance (Shimadzu, AUW120D), followed by calculation of the average mass value and variance. The active mass of each NW electrodes was obtained by mechanical removal from the Pt substrate. The average loading of active mass in the electrodes was found to be 0.00081 g (= 0.81 mg) and had a range of 0.00080−0.00082 g (= 0.80−0.82 mg). A Solartron 1287 electrochemical interface was used to perform the galvanostatic/potentiostatic experiments. Electrochemical impedance experiments utilized the Solartron 1287 electrochemical interface, coupled with a Solartron 1260 frequency response analyzer. Electrochemical impedance spectroscopy was performed in the frequency range from 100 kHz to 10 mHz at a cell potential of 4.77 V (vs Li/Li$^+$) using a signal with an amplitude of 10 mV.

■ RESULTS AND DISCUSSION

Characterization of Nanostructured Electrode Material. The sol−gel-based template synthesis is shown schematically in Figure 1a. Typical morphology of the as-prepared nanowire electrode is observed by SEM (Figure 1b and 1c). From the cross-sectional view of Figure 1c, it is revealed that the nanowires are uniformly protruding from an underlying Pt current collector substrate. The average diameter of each nanowire was determined to be ∼140 nm with a length of approximately 13 μm. The TEM images in Figure 2 detail the
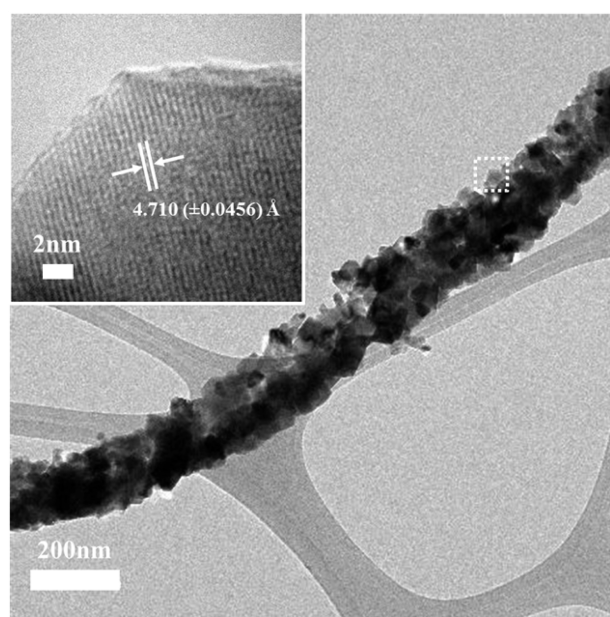

Figure 2. Transmission electron micrographs of LiNi$_{0.5}$Mn$_{1.5}$O$_4$ nanowire electrode prepared via sol−gel based template synthesis method.

fine morphology of the nanowire, which is composed of crystalline particles with an average size of 47 nm and range within 30−80 nm. The particle size was estimated statistically by counting at least 30 different sample regions from the TEM images, followed by calculation of the average size. The nanowires have a polycrystalline structure with nanosize crystallites of different orientations. A legible lattice fringe of 0.47 nm can be observed from the locally magnified TEM images (inset of Figure 2), which is consistent with the (111) interplanar spacing of the disordered structured LiNi$_{0.5}$Mn$_{1.5}$O$_4$. It should be noted again that the nanowire electrodes in this study offer an unbiased ability to study the nanosize effect, as additives to improve electronic conductivity and binding agents have been removed.

The structure of the as-prepared nanowires was characterized using powder X-ray diffraction following mechanical removal from the Pt current collector, as shown in Figure 3. The
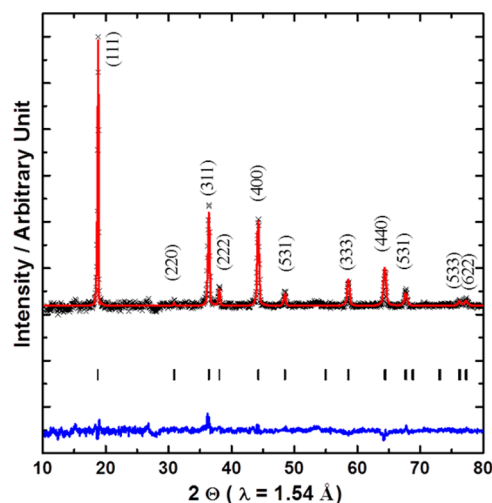

Figure 3. Rietveld refinement results from XRD patterns collected from LiNi$_{0.5}$Mn$_{1.5}$O$_4$ nanowire electrodes. The black crosses represent the observed pattern, the red line corresponds to the calculated diffraction pattern and the blue is the difference pattern.

disordered LiNi$_{0.5}$Mn$_{1.5}$O$_4$ spinel material has a cubic crystal structure with space group $Fd\overline{3}m$. The lithium atoms occupy the tetrahedral sites (Wyckoff position *8a*), while the disordered nickel and manganese atoms occupy the octahedral sties (Wyckoff position *16d*).[35] Rietveld refinement was performed and the refined parameters with reliability factors are presented in Table 1. A relatively high R_b factor was

Table 1. Parameters and Reliability Factors Obtained by the Rietveld Refinement of Nanowire Electrode from Figure 1^a

$a = b = c = 8.192043$ Å, $\alpha = \beta = \gamma = 90°$, $Fd\overline{3}m$ S					
label	atom	X	Y	Z	B	occ
Li1	Li	0.37500	0.37500	0.37500	0.00000	0.96074
Ni1	Ni	0.37500	0.37500	0.37500	0.00000	0.03926
Li2	Li	0.00000	0.00000	0.00000	1.77179	0.03926
Ni2	Ni	0.00000	0.00000	0.00000	1.77179	0.46074
Mn2	Mn	0.00000	0.00000	0.00000	1.77179	1.50000
O3	O	0.24183	0.24183	0.24183	0.00000	4.00000

^{a}Conventional Rietveld reliability factor: $R_{wp} = 3.63$, $R_b = 10.06$

obtained in the refinement, which is likely the result of broadened XRD peak patterns because of nanosize effect.[36] The particle size was calculated to be 41 nm using Scherrer's formula eq 1[36,37] (against the (111) peak; λ = X-ray wavelength, B = full width at half-maximum (fwhm) peak value (Figure S1 in the Supporting Information) and is consistent with the particle size estimated from the TEM images.

Scherrer's Formula

$$L = 0.9\lambda / B \cos \theta \qquad (1)$$

Electrochemical charge and discharge was performed in the potential range of 3.5−4.85 V (vs Li/Li$^+$) with applied current rate of C/7.5 using LiNi$_{0.5}$Mn$_{1.5}$O$_4$ (noncoated) nanowires as the positive electrode (Figure 4a). The plateau at ∼4.7 V (vs
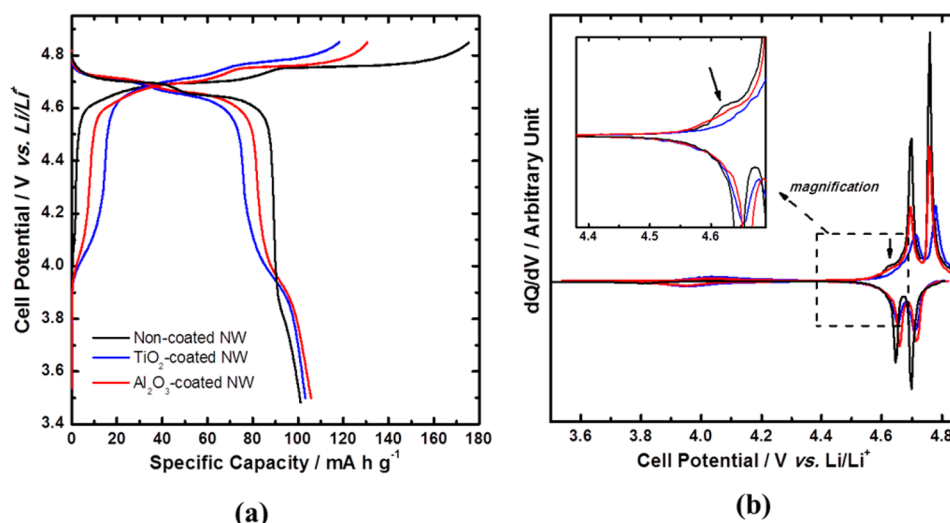
Figure 4. (a) Electrochemical charge and discharge voltage profiles between 3.5−4.85 V (vs Li/Li$^+$) for noncoated nanowire at 1/7.5 C charge and discharge rate (black), and TiO$_2$-coated (blue) and Al$_2$O$_3$-coated (red) nanowires. (b) Differential capacity curves, dQ/dV vs V, of the nanowires.

Li/Li$^+$) arises from the Ni$^{2+/4+}$ redox couple while the plateau at ~4.0 V is the result of the Mn$^{3+/4+}$ couple.

The voltage plateau at ~4.0 V (vs Li/Li$^+$) in the noncoated nanowire shows different behavior than those in the coated nanowires. As shown in Figure 4, it is clear that the overpotential of noncoated nanowires is significantly larger than those of coated nanowires. This is the result of the disparate polarization in as-prepared nanowires. In this study, nanowire electrodes were prepared without carbon and binding additives which leads to poor electrical conductivity and large polarization. This also matches the results of the rate performance test; capacity arising from the voltage plateau at ~4.0 in the fast discharging current density (large polarization) is a lot smaller than that in the slow discharging current density (small polarization) as shown in Supporting Information Figure S7. More specific elementary resistances that contribute to overall polarization can be analyzed in the results of the impedance later. More interestingly, it is also found that charging and discharging curves show a bit different behaviors. This demonstrates an agreement with our previous study, which detailed nonequilibrium structural dynamics in LNMO spinel materials under operando conditions using coherent X-ray diffraction imaging (CXDI). It was reported that a sharp discrepancy exists between electrochemistry and electrode structural changes during a fast charging/discharging process. We discussed that an ionic blockage layer is formed at the surface during fast charging process.[38] Therefore, the electrochemical profile cannot indicate the actual amount of Mn^{3+} in this study. In the previously reported literatures, the origin of Mn(III) ions has been ascribed to transition metal (TM) ion substitutions,[39,40] various crystallization temperatures,[41,42] and different cooling rates[43] during heat treatment. To fix this in the present study, all nanowire electrodes were prepared using the same calcination temperature (800 °C) and cooling rate. Atomic layer deposition is a well-known method which can prevent unpredictable compositional changes during surface deposition on materials due to the low operating temperature. While the electrochemical profiles show similar plateau regions with the typical composite electrodes (with added carbon additive and binder), the irreversible capacity occurs not exclusively in the first cycle, but also in consecutive cycles. It is hypothesized that this is the result of side reactions between the

electrolyte and active electrode material at the electrode/electrolyte interface. By plotting the differential capacity (dQ/dV) vs cell potential (V), a peak is observed above 4.6 V in the first charging profile (Supporting Information Figure S8 details the dQ/dV plot for the first and second charge/discharge cycles), indicating that a side reaction is indeed occurring. This peak is not observed when using conventional powder LiNi$_{0.5}$Mn$_{1.5}$O$_4$ and we purport its evolution to be related to electrode activation. At particularly high potentials, the electrolyte decomposes and forms a layer on the surface of the electrode particles. Previous reports have described that this can be significantly detrimental to lithium-ion conduction through the electrode/electrolyte interface.[37,43] Prolonged operation at high voltage can exacerbate these types of side reactions. In addition, reduction of the manganese(III) ions at the surface of LiNi$_{0.5}$Mn$_{1.5}$O$_4$ leads to manganese(II) ions, which can dissolve in the electrolyte. Manganese(II) ions proceed to diffuse through the electrolyte to the lithium metal anode and plate on the surface.[3,43,44] This leads to an increase in the internal resistance of the cell and as a result, poor battery performance. The particle morphology does not change following electrochemical cycling, but Rietveld refinement shows that the lattice parameter and R_b increase (Figure S2 and S3 in the Supporting Information). This is likely the result of augmentation of the nanosize effect and Mn(II) dissolution. In addition, a recent publication reports structural changes in the electrode during the first cycle, which is been purported to be migration of transition metal ions into empty octahedral sites to form Mn$_3$O$_4$-like and rocksalt-like structures.[45] In the case of LNMO nanowires, the surface area is markedly higher resulting in a large side reaction peak in the charging profile. However, the exact nature of 4.6 V peak in dQ/dV profile in the charging process is still open to debate.

Surface Modification−Atomic Layer Deposition (ALD). To prevent the deleterious effects of electrolyte decomposition and cation dissolution, the interface between the electrolyte and the active materials must be modified. Atomic layer deposition (ALD) is a technology that has been repeatedly shown to be extremely useful in the surface modification of complex nanostructured materials.[29,46] This technique is based on successive, surface-controlled reactions from gaseous reagents to produce thin films and overlayers in
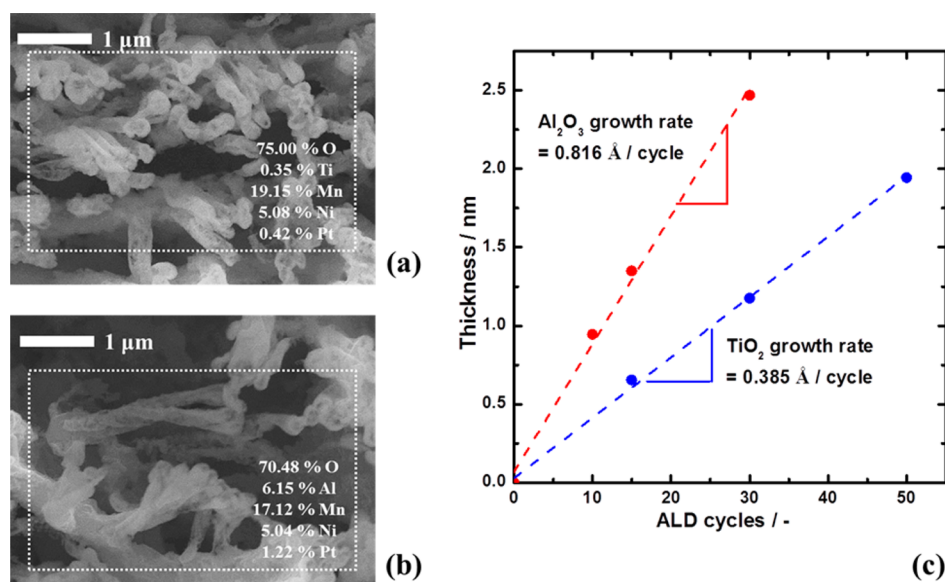
Figure 5. Top views (SEM images) of atomic layer deposition (ALD) coated nanowire electrodes (a) TiO_2 ALD 11 cycles and (b) Al_2O_3 ALD 30 cycles. The insets indicate the percentage of each component from the EDX analysis. (c) Various deposition thickness of the TiO_2 and Al_2O_3 coating layer as a function of ALD cycles.

the nanometer range with perfect conformality and controllability. Figures 5a and 5b show images obtained using SEM as well as energy dispersive X-ray spectroscopy (EDX) analysis of the TiO_2 and Al_2O_3 coated nanowire electrodes. Following successful deposition of TiO_2 and Al_2O_3 thin films, the nanowires were found to be in the same protruding fashion from the Pt substrate. The thickness of the thin film is directly proportional to the number of ALD cycles. The growth rate of both TiO_2 and Al_2O_3 thin films on the nanowire electrodes was calculated as shown in Figure 5c. Each ALD cycle deposits a uniform TiO_2 and Al_2O_3 thin film layer of approximately 0.0389 (= 0.389 Å) and 0.0816 nm (= 0.816 Å) in thickness, respectively, on the nanowire LNMO surface. As shown by TEM (Figure 6a and 6b for TiO_2 and Al_2O_3, respectively), the surface of the coated nanowires is highly smooth and uniform.
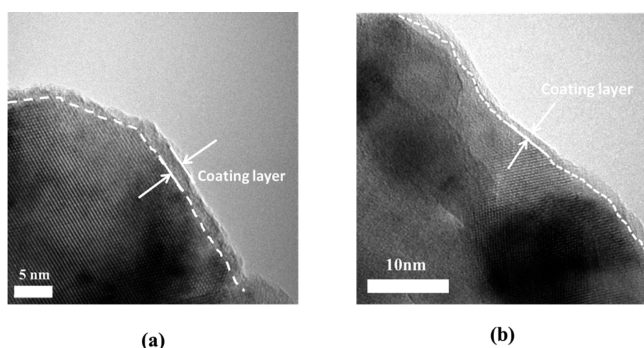

Figure 6. Transmission electron micrographs of (a) TiO_2 ALD-coated (50 ALD cycles) and (b) Al_2O_3 ALD-coated (15 ALD cycles) nanowire.

To determine the effect of the deposition layers on the electrochemical performance of nanowire LNMO electrodes, galvanostatic charge/discharge experiments were performed with an current rate of C/7.5 in the potential range of 3.5−4.85 V (vs Li/Li$^+$).

Figure 4a details a TiO_2-coated nanowire electrode with an approximate coating thickness of 0.43 nm (= 4.3 Å; 11 cycles), and an Al_2O_3-coated nanowire electrode with a coating thickness of ∼0.41 nm (= 4.1 Å; 5 cycles). Electrodes layered with either thin film material were found to exhibit typical redox behavior of $LiNi_{0.5}Mn_{1.5}O_4$, such as the $Ni^{2+/4+}$ and $Mn^{3+/4+}$ plateaus at around 4.7 and 4.0 V (vs Li/Li$^+$), respectively. It was found that the irreversible capacity fade is significantly reduced as a result of coating the nanowire LNMO material using atomic layer deposition.

In spite of the considerable effects of volume and surface area of the nanowire electrode on the electrochemical performance, there is no existing testing method that would allow for the accurate determination of these quantities without damaging the one-dimensional morphology. In lieu of an experimental measurement, the surface area was calculated as follows: as the average diameter of the nanowire is 140 nm (= $2r$) and the length is 13 μm (= L), the outer rectangular area of a nanowire is 5.72×10^{-8} cm^2 (= $2\pi r \times L$). The average number of pores in the polycarbonate (PC) template is 4.7×10^8 pores/cm^2. In addition, the diameter of the electrode cutout is 14 mm, leading to a surface area of 1.54 cm^2 (= $\pi \times 0.7^2$). Hence, the number of nanowires in the electrode is 7.24×10^8 wires (= $4.7 \times 10^8 \times 1.54$), leading to a total outer rectangular area of nanowires to be 41.41 cm^2 (= $(7.24 \times 10^8) \times (5.72 \times 10^{-8})$). Therefore, the total surface of area is 42.95 cm^2 (= 41.41 + 1.54). Using the aforementioned values, the superficial volume of a single nanowire is calculated to be 8.005×10^{-13} cm^3 (=$\pi r^2 \times L$) and the total volume of nanowires is 5.79×10^{-4} cm^3 (= (8.005×10^{-13} cm^3) x (7.24×10^8 wires)). The average thickness of substrate layer is 200 nm, leading to the volume of 0.308×10^{-4} cm^3 (= $1.54(200 \times 10^{-7})$). Therefore, the total volume of electrode is 6.098×10^{-4} cm^3. Accordingly, as shown in Figure 4 (a), the discharge capacity of noncoated NW is 101.12 mAh/g, 134.31 mAh/cm^3, and 1.907×10^{-3} mAh/cm^2. The discharge capacity of the TiO_2-coated electrode is 103.17 mAh/g, 138.73 mAh/cm^3, and 1.969×10^{-3} mAh/cm^2. Nanowire electrodes coated with Al_2O_3 lead to discharge

capacities of 105.72 mAh/g, 140.43 mAh/cm^3, and 1.994 × 10^{-3} mAh/cm^2.

In addition, the electrode/electrolyte side reaction was effectively prevented, as shown by the absence of a peak at ~4.6 V in the differential capacity plot (Figure 4b). Aluminum oxide is a well-known insulating material, and as such it was hypothesized that a thick layer of Al$_2$O$_3$ would inhibit lithium ion movement and dramatically increase the internal resistance. However, the formation of a Li−Al−O film was found to be an effective lithium ion conductor and electronic insulator.[28,47] The surface modification by TiO$_2$ coating is widely adopted to prevent cation dissolution and electrolyte decomposition. However, there are no reports about the lithium ionic conduction mechanism through TiO$_2$ phase. As the thickness of the TiO$_2$ coating layer is less than 0.5 nm, we purport that this TiO$_2$ can form a Li−Ti−O glass phase during the lithiation, analogous to that of Li−Al−O films. This resulted in a retention of electrochemical performance as well as prevention of electrolyte decomposition and manganese ion dissolution.

To further investigate the effect of the ALD coating on the nanowire electrodes, experiments correlating capacity retention with various discharge rates were performed (Figure 7). A cell
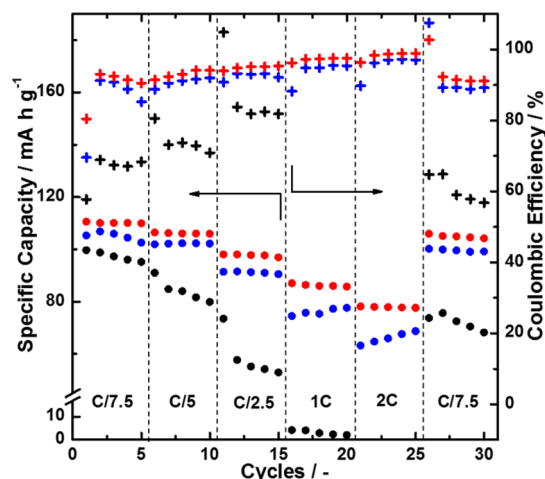

Figure 7. Specific capacity versus cycle number plot at different charge and discharge rates. Black: noncoated NW. Blue: TiO$_2$-coated NW. Red: Al$_2$O$_3$-coated NW.

utilizing a noncoated nanowire electrode shows not merely inferior rate capability (less than 10 mA h g^{-1} at a rate of 1 C), but also significant capacity fading during prolonged cycling. In addition, the Coulombic efficiency was found to be exceptionally poor, dropping to nearly 60% at the 30th cycle. It is postulated that the poor electrochemical performance is a result of increased electrolyte decomposition and cation dissolution associated with the increased active surface area of the nanowires. Coating the nanowire with either TiO$_2$ or Al$_2$O$_3$ resulted in starkly different electrochemical performance compared to noncoated LNMO nanowire electrode. This is exemplified in a much improved observed Coulombic efficiency of >90% at 25th cycle in Figure 7 (e.g., 98.8% in the Al$_2$O$_3$ coated nanowire). In the case of the Al$_2$O$_3$ coated nanowire electrode, the discharging capacity at a 1 C rate still presents 99 mA h g^{-1}.

To probe the effect of surface modification by ALD on the electrochemical reaction mechanism, electrochemical impedance spectroscopy (EIS) measurements were performed in the

charged state at 4.77 V (vs Li/Li$^+$), as shown in Figure 8. These experiments can help to elucidate the elementary resistances
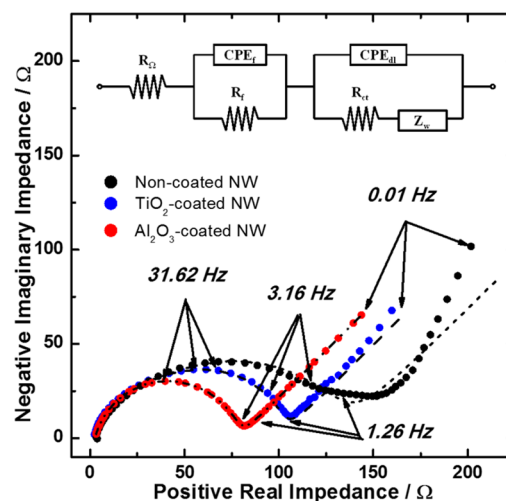

Figure 8. Impedance spectra of nanostructured electrodes, obtained at a cell potential of 4.77 V (vs Li/Li$^+$). The insets are the equivalent circuits to model the reactions in the working and counter electrodes, respectively. Dotted lines were determined from the CNLS fittings of the impedance spectra to the equivalent circuits.

that strongly affect electrochemical performance. The impedance spectra (Nyquist plots) consist of two semicircles: one each in the high and intermediate frequency ranges, and an inclined line at a constant angle to the abscissa. The first semicircle in the high frequency is the result of the lithium migration through the surface film, and the second semicircle in the intermediate frequency originates from the interfacial charge transfer reaction. The inclined line is attributed to solid-state lithium ion diffusion into the active electrode materials. The impedance spectra were modeled using a simplified equivalent circuit as shown in the inset of Figure 8. The resistance, R_Ω, represents the uncompensated ohmic resistance. The first pair of resistance and constant phase element (CPE), R_f-CPE$_f$, indicates that lithium migration occurs through the surface film region. The second pair of resistance and CPE, R_{ct}-CPE$_{ct}$, is indicative of charge-transfer resistance and double layer capacitance. The Warburg impedance, Z_W, describes the solid-state diffusion reaction.[48−50]

All the electrical parameters in the equivalent circuit were determined from the CNLS (complex nonlinear least-squares) fitting method,[34,51,52] and are summarized in the Table 2. It is particularly noteworthy that the resistance R_f from the TiO$_2$ and Al$_2$O$_3$ coated nanowires, reduced by about 50 and 70 Ω, respectively. This corresponds to a reduction of approximately 44% and 67% when compared to that of the noncoated nanowire electrode. Impedance spectroscopy results indicate that the resistance originating from the surface film region in the charged state (4.77 V vs Li/Li$^+$) can be significantly reduced by ALD coating on the active materials. A reduction in resistance suggests that electrolyte decomposition at high voltage operation and manganese ion dissolution have been curtailed.

To investigate the extent of cation dissolution into the electrolyte, the electrochemical cells were disassembled in an argon filled glovebox and the electrolyte was separated from the other battery components. Elemental analysis of the electrolyte was performed using inductively coupled plasma optical

Table 2. Electrical Parameters of the Working Electrodes, Determined from the Complex Nonlinear Least Squares (CNLS) Fitting of Impedance Spectra to the Equivalent Circuit[a]

	Positive electrode								
				CPE$_f$			CPE$_{dl}$		
	Cell potential	R$_\Omega$	R$_f$	C		R$_{ct}$	C		A$_\omega$
	V (vs Li/Li$^+$)	Ω	Ω	mF s$^{\eta-1}$	η	Ω	μF s$^{\eta-1}$	η	Ω s$^{-0.5}$
Bare NW	4.77	2.82	105	0.295	0.751	24.37	96.5	0.888	30.29
TiO$_2$ ALD		2.06	58.99	0.158	0.923	39.66	77.5	0.862	25.11
Al$_2$O$_3$ ALD		2.57	34.14	0.108	0.823	41.93	56.9	0.871	23.10

[a]This also includes the diffusion coefficient, diffusion length, and some calculated values.

emission spectrometry (ICP-OES). It was found that manganese ion dissolution into the electrolyte is alleviated when electrodes are coated with either TiO$_2$ or Al$_2$O$_3$ (Figure 9a). The concentration of manganese in the electrolyte when
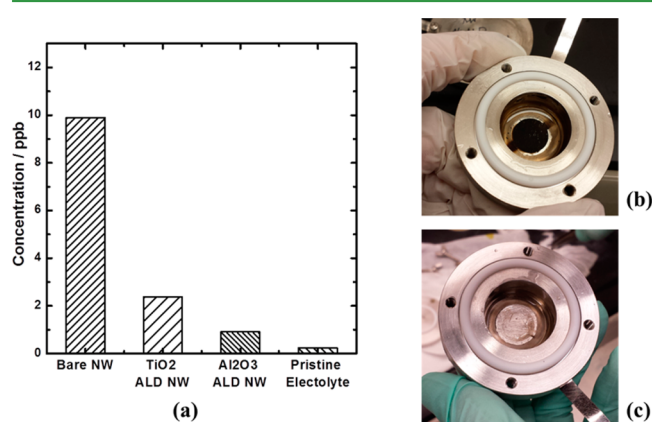

Figure 9. (a) Mn dissolution into the electrolytes with the nanowire electrodes from ICP-OES analysis. Photographs of Li counter electrodes after the electrochemical tests (b) without ALD (bare nanowire) and (c) with Al$_2$O$_3$ ALD.

using noncoated LNMO electrode was determined to be ~10 ppb after 30 cycles of electrochemical charging and discharging. However, when the nanowires are coated with Al$_2$O$_3$ (5 ALD cycles, ~4 nm thickness), the concentration of manganese in the electrolyte decreased to a mere ~1 ppb. Increased cation dissolution was found to result in severe darkening of the lithium metal anode. However, cells using an aluminum oxide coated LMNO cathode resulted in a relatively clean and shiny lithium anode surface. This qualitative observation further reveals how significant a reduction in Mn(II) dissolution results when coating the nanowires with insulating thin films.

CONCLUSION

Our studies have indicated that an increase in surface area of one-dimensional nanowire electrode results in detrimental interfacial side reactions. Protective thin films composed of either titanium dioxide or aluminum oxide were successfully deposited on LNMO nanowire electrodes using atomic layer deposition. The protective layer at the surface of the nanowire makes it possible to not merely decrease the irreversible capacity fade but also diminish the manganese dissolution during electrochemical cycling. This results in an acceleration of lithium ion migration through the surface film and a reduction in resistance. Our work gives significant insight in the importance of interface protection for high voltage nano-structured electrode materials.

ASSOCIATED CONTENT

ⓢ Supporting Information

Particle size calculation from the Scherrer equation, Rietveld refinement results, XRD and SEM before and after the electrochemical cycles, electrochemical voltage profiles with various ALD coating thickness and applied currents, differential capacity (dQ/dV). The Supporting Information is available free of charge on the ACS Publications website at DOI: 10.1021/acsami.5b01392.

AUTHOR INFORMATION

Corresponding Author
*Tel: +1 858 822 4247. Fax: +1 858 534 9553. E-mail: shmeng@ucsd.edu.

Notes

The authors declare no competing financial interest.

ACKNOWLEDGMENTS

REFERENCES

(1) Whittingham, M. S. Lithium Batteries and Cathode Materials. *Chem. Rev.* **2004**, *104*, 4271−4302.
(2) Manthiram, A.; Chemelewski, K.; Lee, E.-S. A Perspective on the High-Voltage LiMn1.5Ni0.5O4 Spinel Cathode for Lithium-Ion Batteries. *Energy Environ. Sci.* **2014**, *7*, 1339−1350.
(3) Xiao, J.; Chen, X.; Sushko, P. V.; Sushko, M. L.; Kovarik, L.; Feng, J.; Deng, Z.; Zheng, J.; Graff, G. L.; Nie, Z.; Choi, D.; Liu, J.; Zhang, J.-G.; Whittingham, M. S. High-Performance LiNi0.5Mn1.5O4 Spinel Controlled by Mn3+ Concentration and Site Disorder. *Adv. Mater.* **2012**, *24*, 2109−2116.
(4) Dunn, B.; Liu, P.; Meng, S. Nanoscience and Nanotechnology in Next Generation Lithium Batteries. *Nanotechnology* **2013**, *24*, 420201.
(5) Jiang, J.; Li, Y.; Liu, J.; Huang, X.; Yuan, C.; Lou, X. W. Recent Advances in Metal Oxide-based Electrode Architecture Design for Electrochemical Energy Storage. *Adv. Mater.* **2012**, *24* (38), 5166−5180.
(6) Pitchai, R.; Thavasi, V.; Mhaisalkar, S. G.; Ramakrishna, S. Nanostructured Cathode Materials: a Key for Better Performance in Li-Ion Batteries. *J. Mater. Chem.* **2011**, *21*, 11040−11051.
(7) Lee, K. T.; Cho, J. Roles of Nanosize in Lithium Reactive Nanomaterials for Lithium Ion Batteries. *Nano Today* **2011**, *6*, 28−41.
(8) Song, H.-K.; Lee, K. T.; Kim, M. G.; Nazar, L. F.; Cho, J. Recent Progress in Nanostructured Cathode Materials for Lithium Secondary Batteries. *Adv. Funct. Mater.* **2010**, *20*, 3818−3834.

(9) Aurbach, D., The Role of Surface Films on Electrodes in Li-Ion Batteries. In *Advances in Lithium-Ion Batteries*; Schalkwijk, W., Scrosati, B., Eds.; Kluwer: New York, 2002; pp 7−77.

(10) Lee, J.-W.; Park, S.-J.; Choi, W.-S.; Shin, H.-C. Well-Defined Meso- to Macro-Porous Film of Tin Oxides Formed by an Anodization Process. *Electrochim. Acta* 2011, *56*, 5919−5925.

(11) Jung, H.-R.; Kim, E.-J.; Park, Y. J.; Shin, H.-C. Nickel-Tin Foam with Nanostructured Walls for Rechargeable Lithium Battery. *J. Power Sources* 2011, *196*, 5122−5127.

(12) Liu, H.; Cho, H.-M.; Meng, Y. S.; Li, Q. Engineering Three-Dimensionally Electrodeposited Si-on-Ni Inverse Opal Structure for High Volumetric Capacity Li-Ion Microbattery Anode. *ACS Appl. Mater. Interfaces* 2014, *6*, 9842−9849.

(13) Wang, L.; He, X.; Sun, W.; Wang, J.; Li, Y.; Fan, S. Crystal Orientation Tuning of LiFePO4 Nanoplates for High Rate Lithium Battery Cathode Materials. *Nano Lett.* 2012, *12*, 5632−5636.

(14) Wang, J.; Yang, J.; Tang, Y.; Li, R.; Liang, G.; Sham, T.-K.; Sun, X. Surface Aging at Olivine LiFePO4: a Direct Visual Observation of Iron Dissolution and the Protection Role of Nano-Carbon Coating. *J. Mater. Chem. A* 2013, *1*, 1579−1586.

(15) Hao, X.; Bartlett, B. M. Improving the Electrochemical Stability of the High-Voltage Li-Ion Battery Cathode LiNi0.5Mn1.5O4 by Titanate-Based Surface Modification. *J. Electrochem. Soc.* 2013, *160*, A3162−A3170.

(16) Cheng, H.-M.; Wang, F.-M.; Chu, J. P.; Santhanam, R.; Rick, J.; Lo, S.-C. Enhanced Cycleabity in Lithium Ion Batteries: Resulting from Atomic Layer Depostion of Al2O3 or TiO2 on LiCoO2 Electrodes. *J. Phys. Chem. C* 2012, *116*, 7629−7637.

(17) Deng, H.; Nie, P.; Luo, H.; Zhang, Y.; Wang, J.; Zhang, X. Highly Enhanced Lithium Storage Capability of LiNi0.5Mn1.5O4 by Coating with Li2TiO3 for Li-Ion Batteries. *J. Mater. Chem. A* 2014, *2*, 18256−18262.

(18) Konishi, H.; Suzuki, K.; Taminato, S.; Kim, K.; Zheng, Y.; Kim, S.; Lim, J.; Hirayama, M.; Son, J.-Y.; Cui, Y.; Kanno, R. Effect of Surface Li3PO4 Coating on LiNi0.5Mn1.5O4 Epitaxial Thin Film Electrodes Synthesized by Pulsed Laser Deposition. *J. Power Sources* 2014, *269*, 293−298.

(19) Li, X.; Guo, W.; Liu, Y.; He, W.; Xiao, Z. Spinel LiNi0.5Mn1.5O4 as Superior Electrode Materials for Lithium-Ion Batteries: Ionic Liquid Assisted Synthesis and the Effect of CuO Coating. *Electrochim. Acta* 2014, *116*, 278−283.

(20) Song, J.; Han, X.; Gaskell, K.; Xu, K.; Lee, S.; Hu, L. Enhanced Electrochemical Stability of High-Voltage LiNi0.5Mn1.5O4 Cathode by Surface Modification using Atomic Layer Deposition. *J. Nanopart. Res.* 2014, *16*, 1−8.

(21) Xiao, X.; Ahn, D.; Liu, Z.; Kim, J.-H.; Lu, P. Atomic Layer Coating to Mitigate Capacity Fading Associated with Manganese Dissolution in Lithium Ion Batteries. *Electrochem. Commun.* 2013, *32*, 31−34.

(22) Park, J. S.; Meng, X.; Elam, J. W.; Hao, S.; Wolverton, C.; Kim, C.; Cabana, J. Ultrathin Lithium-Ion Conducting Coatings for Increased Interfacial Stability in High Voltage Lithium-Ion Batteries. *Chem. Mater.* 2014, *26*, 3128−3134.

(23) Zhang, Q.; Mei, J.; Wang, X.; Tang, F.; Fan, W.; Lu, W. High Performance Spinel LiNi0.5Mn1.5O4 Cathode Material by Lithium Polyacrylate Coating for Lithium Ion Battery. *Electrochim. Acta* 2014, *143*, 265−271.

(24) Gao, X.-W.; Deng, Y.-F.; Wexler, D.; Chen, G.-H.; Chou, S.-L.; Liu, H.-K.; Shi, Z.-C.; Wang, J.-Z. Improving the Electrochemical Performance of the LiNi0.5Mn1.5O4 Spinel by Polypyrrole Coating as a Cathode Material for the Lithium-Ion Battery. *J. Mater. Chem. A* 2015, *3*, 404−411.

(25) Niketic, S.; Couillard, M.; MacNeil, D.; Abu-Lebdeh, Y. Improving the Performance of High Voltage LiMn1.5Ni0.5O4 Cathode Material by Carbon Coating. *J. Power Sources* 2014, *271*, 285−290.

(26) Kim, J. W.; Travis, J. J.; Hu, E.; Nam, K.-W.; Kim, S. C.; Kang, C. S.; Woo, J.-H.; Yang, X.-Q.; George, S. M.; Oh, K. H.; Cho, S.-J.; Lee, S.-H. Unexpected High Power Performance of Atomic Layer

Deposition Coated Li[Ni1/3Mn1/3Co1/3]O2 Cathodes. *J. Power Sources* 2014, *254*, 190−197.

(27) Ban, C.; Xie, M.; Sun, X.; Travis, J. J.; Wang, G.; Sun, H.; Dillon, A. C.; Lian, J.; George, S. M. Atomic Layer Deposition of Amorphous TiO 2 on Graphene as an Anode for Li-Ion Batteries. *Nanotechnology* 2013, *24*, 424002.

(28) Nguyen, H. T.; Zamfir, M. R.; Duong, L. D.; Lee, Y. H.; Bondavalli, P.; Pribat, D. Alumina-Coated Silicon-Based Nanowire Arrays for High Quality Li-Ion Battery Anodes. *J. Mater. Chem.* 2012, *22*, 24618−24626.

(29) Marichy, C.; Bechelany, M.; Pinna, N. Atomic Layer Deposition of Nanostructured Materials for Energy and Environmental Applications. *Adv. Mater.* 2012, *24*, 1017−1032.

(30) Scott, I. D.; Jung, Y. S.; Cavanagh, A. S.; Yan, Y.; Dillon, A. C.; George, S. M.; Lee, S.-H. Ultrathin Coatings on Nano-LiCoO2 for Li-Ion Vehicular Applications. *Nano Lett.* 2011, *11*, 414−418.

(31) Sides, C. R.; Martin, C. R., Nanomaterials in Li-Ion Battery Electrode Design. In *Modern Aspects of Electrochemistry*, No. 40; White, R. E., Vayenas, C. G., Gamboa-Aldeco, M. E., Eds.; Springer: New York, 2007; Chapter 3, p 75.

(32) Cho, H.-M.; Meng, Y. S. Effect of Ni/Mn Ordering on Elementary Polarizations of LiNi0.5Mn1.5O4 Spinel and Its Nano-structured Electrode. *J. Electrochem. Soc.* 2013, *160*, A1482−A1488.

(33) Cho, H. M.; Park, Y. J.; Shin, H. C. Semiempirical Analysis of Time-Dependent Elementary Polarizations in Electrochemical Cells. *J. Electrochem. Soc.* 2010, *157*, A8−A18.

(34) Cho, H. M.; Shin, H. C., Analysis of Cell Impedance for the Design of a High-Power Lithium-Ion Battery In *Lithium Batteries Research, Technology, and Applications*; Dahlin, G. R., Strom, K. E., Eds.; Nova Science Publishers: New York, 2010; pp 73−118.

(35) Kim, J. H.; Myung, S. T.; Yoon, C. S.; Kang, S. G.; Sun, Y. K. Comparative Study of LiNi0.5Mn1.5O4-δ and LiNi0.5Mn1.5O4 Cathodes Having Two Crystallographic Structures: Fd3̄m and P4332. *Chem. Mater.* 2004, *16*, 906−914.

(36) Cullity, B. D. *Elements of X-ray Diffraction*; Addison-Wesley Pub. Co.: Reading, MA, 1956.

(37) Liu, D.; Zhu, W.; Trottier, J.; Gagnon, C.; Barray, F.; Guerfi, A.; Mauger, A.; Groult, H.; Julien, C. M.; Goodenough, J. B.; Zaghib, K. Spinel Materials for High-Voltage Cathodes in Li-Ion Batteries. *RSC Adv.* 2014, *4*, 154−167.

(38) Singer, A.; Ulvestad, A.; Cho, H.-M.; Kim, J. W.; Maser, J.; Harder, R.; Meng, Y. S.; Shpyrko, O. G. Nonequilibrium Structural Dynamics of Nanoparticles in LiNi1/2Mn3/2O4 Cathode under Operando Conditions. *Nano Lett.* 2014, *14*, 5295−5300.

(39) Liu, J.; Manthiram, A. Understanding the Improved Electro-chemical Performances of Fe-Substituted 5 V Spinel Cathode LiMn1.5Ni0.5O4. *J. Phys. Chem. C* 2009, *113*, 15073−15079.

(40) Yang, M.-C.; Xu, B.; Cheng, J.-H.; Pan, C.-J.; Hwang, B.-J.; Meng, Y. S. Electronic, Structural, and Electrochemical Properties of LiNixCuyMn2−x−yO4 (0 < x < 0.5, 0 < y < 0.5) High-Voltage Spinel Materials. *Chem. Mater.* 2011, *23*, 2832−2841.

(41) Sun, Y.; Yang, Y.; Zhan, H.; Shao, H.; Zhou, Y. Synthesis of High Power Type LiMn1.5Ni0.5O4 by Optimizing Its Preparation Conditions. *J. Power Sources* 2010, *195*, 4322−4326.

(42) Cabana, J.; Casas-Cabanas, M.; Omenya, F. O.; Chernova, N. A.; Zeng, D.; Whittingham, M. S.; Grey, C. P. Composition-Structure Relationships in the Li-Ion Battery Electrode Material LiNi0.5Mn1.5O4. *Chem. Mater.* 2012, *24*, 2952−2964.

(43) Song, J.; Shin, D. W.; Lu, Y.; Amos, C. D.; Manthiram, A.; Goodenough, J. B. Role of Oxygen Vacancies on the Performance of Li[Ni0.5−xMn1.5+x]O4 (x = 0, 0.05, and 0.08) Spinel Cathodes for Lithium-Ion Batteries. *Chem. Mater.* 2012, *24*, 3101−3109.

(44) Zhong, G. B.; Wang, Y. Y.; Yu, Y. Q.; Chen, C. H. Electrochemical Investigations of the LiNi0.45M0.10Mn1.45O4 (M = Fe, Co, Cr) 5V Cathode Materials for Lithium Ion Batteries. *J. Power Sources* 2012, *205*, 385−393.

(45) Lin, M.; Ben, L.; Sun, Y.; Wang, H.; Yang, Z.; Gu, L.; Yu, X.; Yang, X.-Q.; Zhao, H.; Yu, R.; Armand, M.; Huang, X. Insight into the

Atomic Structure of High-Voltage Spinel LiNi0.5Mn1.5O4 Cathode Material in the First Cycle. *Chem. Mater.* **2015**, *27*, 292−303.

(46) Knez, M.; Nielsch, K.; Niinistö, L. Synthesis and Surface Engineering of Complex Nanostructures by Atomic Layer Deposition. *Adv. Mater.* **2007**, *19*, 3425−3438.

(47) Liu, Y.; Hudak, N. S.; Huber, D. L.; Limmer, S. J.; Sullivan, J. P.; Huang, J. Y. In Situ Transmission Electron Microscopy Observation of Pulverization of Aluminum Nanowires and Evolution of the Thin Surface Al2O3 Layers during Lithiation−Delithiation Cycles. *Nano Lett.* **2011**, *11*, 4188−4194.

(48) Levi, M. D.; Aurbach, D. Simultaneous Measurements and Modeling of the Electrochemical Impedance and the Cyclic Voltammetric Characteristics of Graphite Electrodes Doped with Lithium. *J. Phys. Chem. B* **1997**, *101*, 4630−4640.

(49) Levi, M. D.; Salitra, G.; Markovsky, B.; Teller, H.; Aurbach, D.; Heider, U.; Heider, L. Solid-State Electrochemical Kinetics of Li-Ion Intercalation into Li1-xCoO2: Simultaneous Application of Electro-analytical Techniques SSCV, PITT, and EIS. *J. Electrochem. Soc.* **1999**, *146*, 1279−1289.

(50) Barsoukov, E.; Macdonald, J. R. *Impedance Spectroscopy: Theory, Experiment, and Applications*, 2nd ed.; Wiley-Interscience: Hoboken, NJ, 2005.

(51) Huang, Q.-A.; Hui, R.; Wang, B.; Zhang, J. A Review of AC Impedance Modeling and Validation in SOFC Diagnosis. *Electrochim. Acta* **2007**, *52*, 8144−8164.

(52) Schichlein, H.; Müller, A. C.; Voigts, M.; Krügel, A.; Ivers-Tiffée, E. Deconvolution of Electrochemical Impedance Spectra for the Identification of Electrode Reaction Mechanisms in Solid Oxide Fuel Cells. *J. Appl. Electrochem.* **2002**, *32*, 875−882.